ARCHIVES OF ACOUSTICS
36, 4, 927–935 (2011)

DOI: 10.2478/v10168-011-0062-4

Synthetic Aperture Technique Applied to Tissue Attenuation Imaging

Ziemowit KLIMONDA, Jerzy LITNIEWSKI, Andrzej NOWICKI

Department of Ultrasound
Institute of Fundamental Technological Research
Polish Academy of Sciences
Pawińskiego 5B, 02-106 Warszawa, Poland
e-mail: zklim@ippt.gov.pl

(*received October 13, 2011; accepted November 16, 2011*)

The attenuating properties of biological tissue are of great importance in ultrasonic medical imaging. Investigations performed *in vitro* and *in vivo* showed the correlation between pathological changes in the tissue and variation of the attenuation coefficient. In order to estimate the attenuation we have used the downshift of mean frequency (f_m) of the interrogating ultrasonic pulse propagating in the medium. To determine the f_m along the propagation path we have applied the f_m estimator (I/Q algorithm adopted from the Doppler mean frequency estimation technique). The mean-frequency shift trend was calculated using Single Spectrum Analysis. Next, the trends were converted into attenuation coefficient distributions and finally the parametric images were computed. The RF data were collected in simulations and experiments applying the synthetic aperture (SA) transmit-receiving scheme. In measurements the ultrasonic scanner enabling a full control of the transmission and reception was used. The resolution and accuracy of the method was verified using tissue mimicking phantom with uniform echogenicity but varying attenuation coefficient.

Keywords: tissue attenuation imaging, synthetic aperture, diagnosis enhancing.

1. Introduction

The attenuating properties of biological tissue are of great importance in ultrasonic medical imaging. It has been emphasized in many publications that ultrasound attenuation is closely related to the type and pathological state of the tissue. Investigations performed *in vitro* and *in vivo* showed the correlations between pathological changes in the tissue and variation of the attenuation coefficient. Liver is the most frequent example. The *in vivo* characterization of this

organ is often restricted to its attenuation properties and it has been proved that the ultrasonic attenuation coefficient increases as the amount of pathological fat in the liver increases (Oosterveld *et al.*, 1991; Lu *et al.*, 1999). Also, the study of excised cancer tissue revealed the differences in acoustic attenuation among cancer types and degrees of pathology. Saijo and Sasaki (1996) employed scanning acoustic microscope to measure five types of gastric cancer and indicated different attenuation coefficient and sound speed comparing to normal tissue. Bigelow *et al.* (2008) and McFarlin *et al.* (2010) investigated possibility of the prediction of the premature delivery based on the noninvasive ultrasonic attenuation determination in rats and in humans respectively. Worthington and Shear (2001) presented that thermal coagulation of porcine kidney changes attenuation and Zderic *et al.* (2004) demonstrated strong attenuation changes in porcine liver related with HIFU treatment.

The long term goal of this study is to develop the attenuation parametric imaging technique and to apply it for *in vivo* characterization of tissue.

2. Attenuation determination

When a wideband ultrasonic pulse with mean frequency f_0, propagates within the homogenous medium the dispersion of the attenuation coefficient results in the shift of the pulse mean frequency. The new mean frequency f_m can be expressed by (Laugier *et al.*, 1985; Litniewski, 2006):

$$f_m = f_0 - \sigma^2 \alpha_0 x. \tag{1}$$

The σ^2 is the Gaussian variance of the pulse spectrum, x denotes penetrated distance and α_0 is the attenuation coefficient. Gaussian pulse spectrum preserves the shape during propagation in linearly attenuating medium i.e. the σ^2 is constant.

The f_m was estimated using the estimator I/Q algorithm, called sometimes the correlation estimator. The estimator is depicted by

$$f_m = \frac{1}{2\pi T_s} \arctan \left(\frac{\sum_{i=1}^{N} Q(i)I(i+1) - Q(i+1)I(i)}{\sum_{i=1}^{N} I(i)I(i+1) + Q(i+1)Q(i)} \right), \tag{2}$$

where T_s is the sampling period, i is the sample number and N is the estimator window length. The Q and I are quadrature and in-phase signal components and are obtained by quadrature sampling technique. The N parameter is directly related to the axial resolution of the method (Klimonda *et al.*, 2009). The f_m line is created point by point from the raw backscattered RF data.

The f_m distribution lines are characterized by high variance due to random character of signal backscattered in soft tissue. The reduction of the f_m

line random variability was realized by the moving average filtration and the Singular Spectrum Analysis (SSA) technique (Hassani, 2007). The SSA trend extraction algorithm operates along the f_m lines in axial direction. The SSA is relatively new technique of analysis of the time series. The aim of this technique is the decomposition of the input data series into the sum of components which can be interpreted as the trend, oscillatory components and the noise (non-oscillatory components). The major application of the SSA technique is the smoothing of the time series, finding the trend, forecasting and detection of the structural changes. The final attenuation estimates were enumerated from the smoothed f_m lines. The application of the SSA and the averaging of the scan lines limit the variations of the attenuation estimate but it is still affected by errors.

3. Synthetic Aperture technique

The synthetic aperture methods (SA) are widely used in radar techniques (Curlander, McDonough, 1991). The implementation of SA technique in medical ultrasound systems with multi-elements probe is also possible. The idea of using SA technique for acquiring RF data that are next processed for attenuation determination is twofold. We know that focusing introduce variation of pulse spectrum what results in incorrect assessment of attenuation. This focusing effect must be compensated (Litniewski *et al.*, 2009). For standard delay and sum (DAS) beamforming the focusing is performed only in several, fixed distances in the tissue. Thus the influence of focusing varies along the echo line. In case of SA technique the focusing is performed in all points of imaged tissue and its influence on the mean frequency of the signal is very similar in the whole imaging area. Thus the correction of focusing effects is much simpler and more effective when SA imaging is applied rather then standard DAS beamforming is used. Also, the attenuation imaging requires application of averaging over adjacent echo lines in lateral direction and axially along the line, reducing however the spatial resolution of attenuation images. In a case of SA the averaging is much more effective because the areas in the vicinity of focus are statistically independent and averaging over only few of them is required to reduce stochastic factors in calculated attenuation. Out of the focus (the case for most of the imaging area when the standard beamforming is used) the areas insonificated by adjacent beams are overlapping and more averaging is required worsening the resolution of attenuation map. There are plenty of transmission-reception schemes used in SA techniques. In this paper, we used basic Synthetic Transmit Aperture (STA) scheme. The idea of the scheme is presented in Fig. 1. This scheme is carried out by sequential transmitting with one transducer and receiving with all transducer until the full aperture scan is performed.

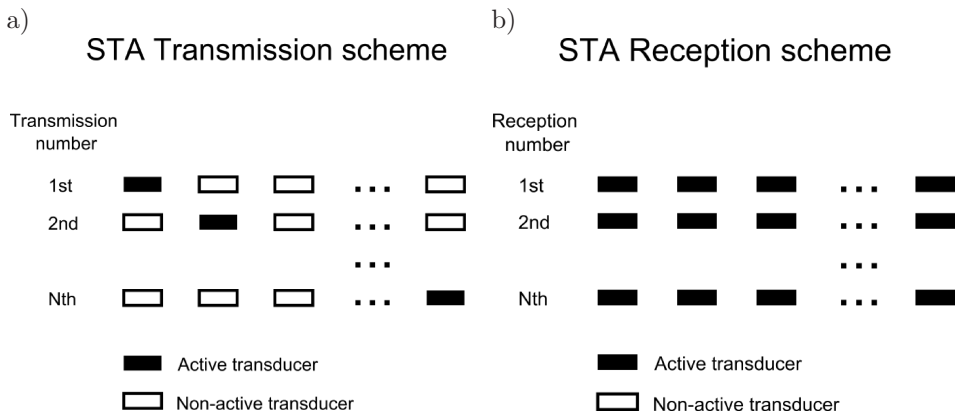

Fig. 1. Basic STA transmission (a) and reception (b) schemes for linear aperture consisted of N transducers.

4. Simulation

The idea of applying the synthetic aperture technique to collect the ultrasonic echoes from the tissue and subsequently to estimate the tissue attenuation was evaluated using FieldII software – a program that applies the linear acoustics for the simulation of the pressure fields/beams and resulting backscattering fields emitted and received by linear, convex and phase array transducers (Jensen, Svendsen, 1992; Jensen, 1996). FieldII considers the media with uniform distribution of attenuation coefficient only. We have introduced the following procedure to simulate the waves scattered in the attenuating medium that contains objects of different attenuation. Let's consider the tissue mimicking phantom with point scatterers r randomly distributed in attenuating background medium (background attenuation coefficient $\alpha_b = 0.5$ dB/(MHz·cm)) and in the cylindrical object (object attenuation coefficient $\alpha_{ob} = 0.9$ dB/(MHz·cm), 15 mm diameter) embedded in the medium at 30 mm depth (Fig. 2). The constant tis-

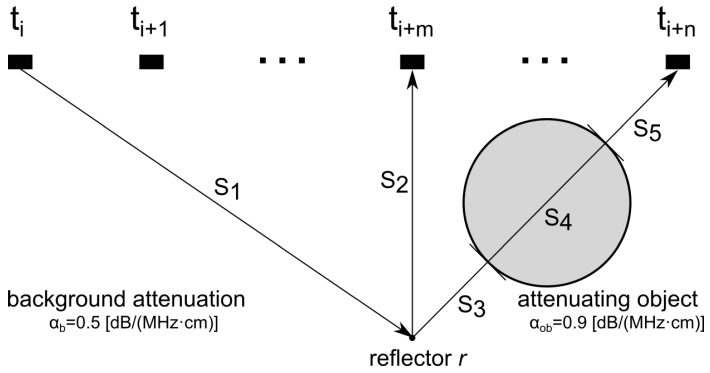

Fig. 2. The wave propagation paths used for the simulations of the transducers responses to the wave scattered in the medium with attenuating object.

sue density and sound velocity were assumed both in the cylinder and in the surrounding medium. $N = 64$ elements linear array was used in the simulation. The response of each receiving-transducer to the wavelet scattered on each scatterer and emitted by each transmitting transducer must be calculated. For simplification let's assume that only one transducer t_i emits the wavelet that is scattered by one scatterer r and we look for the responses from t_{i+m} and t_{i+n} transducers (Fig. 2). The wavelet emitted by the transducer t_i propagates to the reflector and next to the transducer t_{i+m} along the path segments labeled as S_1 and S_2. The response of transducer t_{i+m} is simulated by FieldII assuming that the attenuation is constant along the propagation path.

The wavelet emitted by the transducer t_i and received by the transducer t_{i+n} propagates along the path segments labeled as S_1, S_3, S_4 and S_5. The S_4 path segment corresponds to the wave propagation in the object with increased attenuation. The response of transducer t_{i+n} can be simulated by FieldII assuming the constant attenuation α_{average}, averaged along all path segments from t_i to t_{i+n}. The α_{average} is given by Eq. (3)

$$\alpha_{\text{average}} = \alpha_b \cdot \left(\frac{S_1 + S_3 + S_5}{S_1 + S_3 + S_4 + S_5} \right) + \alpha_{ob} \cdot \left(\frac{S_4}{S_1 + S_3 + S_4 + S_5} \right). \tag{3}$$

The average attenuation was calculated separately and was implemented into the FieldII software. The transmitting and receiving transducers (t_i and t_j), form the transmit-receive transducer pair T_{ij}. The final backscattered RF signal P for a T_{ij} is the sum of all component signals p simulated for all reflectors r_k and is described by Eq. (4):

$$P(T_{ij}) = \sum_{k=1}^{N} p(T_{ij}, r_k). \tag{4}$$

In the simulation we have used 64-elements linear array, 5 MHz center frequency. The height, width and pitch of the transducers were 4, 0.38 and 0.48 mm, respectively and corresponded to the geometry of the ultrasonic probe used in the experiment.

In the experiments 128-elements linear array was used, while, as it was pointed out previously, the simulated probe was assumed to consist 64 elements only, to keep the computation time and computer memory usage at acceptable level. The simulated RF data were processed by STA algorithms and the final RF echoes were obtained. The mean frequency estimate, which is the base of the attenuation estimate, is affected by the diffraction effects, particularly when determine close to the transducer. The diffraction compensation function was calculated numerically as follows. The impulse response of the system, assuming non attenuating medium was simulated for each point of the imaged region using FieldII. Next, the average frequency of the impulse response was calculated and the frequency distribution map was obtained. Then, this frequency map was subtracted from the mean frequency distribution obtained in the phantom simu-

lation. The corrected mean frequency distribution was next processed as depicted in "Attenuation Determination" section. The resulting images are presented in Fig. 3. While the attenuating object cannot be detected on the standard B-scan (Fig. 3a), the attenuation distribution image is clearly visible (Fig. 3b). The estimated mean attenuation value of the imaged object equals 0.83 dB/(MHz·cm), thus it is very close to the simulated attenuation value.

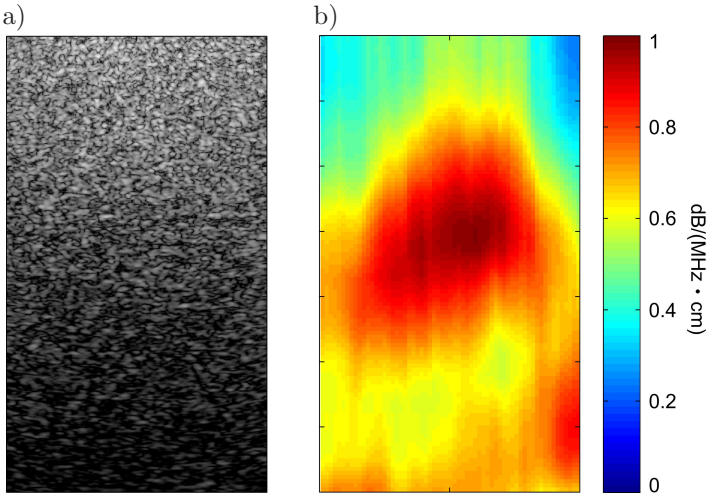

Fig. 3. The B-scan (a) and the attenuation distribution image (b) of the simulated attenuating cylinder (0.9 dB/(MHz·cm)) immersed in less attenuating medium (0.5 dB/(MHz·cm)). Imaging area 20 mm × 35 mm.

5. Measurements

The experimental data were recorded using ultrasonic scanner (Ultrasonix Sonic TOUCH) equipped with linear array probe (128 elements) and operating at 7.0 MHz frequency. The system enables a full control of the transmission and reception giving the access to every single piezo-element of multi-elements ultrasonic probe. The RF data were collected applying basic STA scheme with one element transmitting and all elements receipting. Next the data were processed and attenuation map was created. The resolution and accuracy of the method was verified using tissue mimicking phantom (Dansk Fantom Service) with uniform echogenicity but varying attenuation coefficient. The phantom consists of two cylinders of 15 mm diameter with attenuation coefficient equal to 0.9 and 0.7 dB/(MHz·cm) respectively, that were embedded in the medium with attenuation of 0.5 dB/(MHz·cm) at the depth of approximately 30 mm. The diffraction correction and calibration were performed using reference phantom with uniform attenuation equal 0.5 dB/(MHz·cm). The images obtained by using SA technique and Sonic TOUCH system are presented in Figs. 4 and 5. The objects are invisible in B-mode and clearly visible in attenuation images.

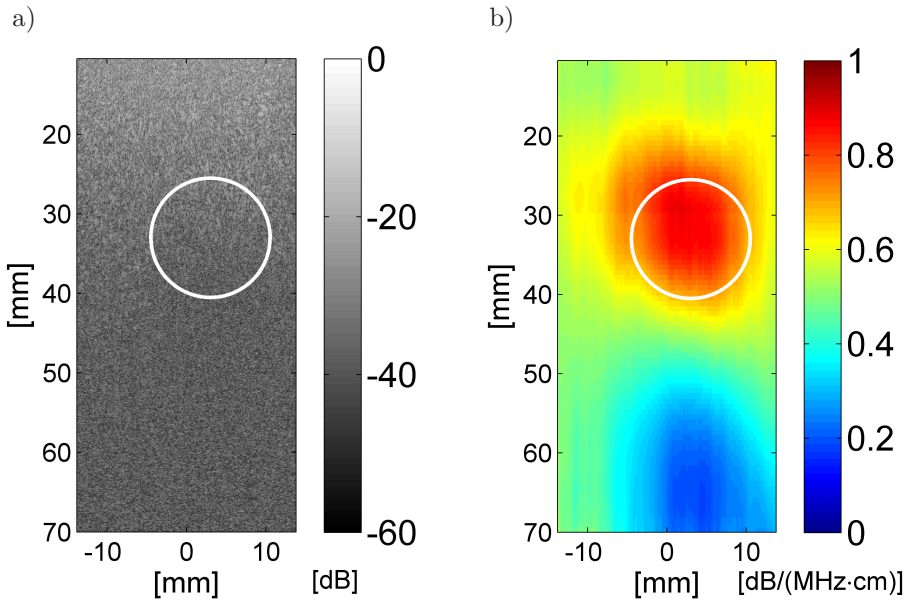

Fig. 4. B-scan image of the cylinder (attenuation 0.9 dB/MHz·cm) (a) and its attenuation distribution image (b). The white circles mark the real positions of cylinders. The shadows beneath the objects are artifacts and are caused by decreased signal-to-noise ratio (SNR) of echoes, due to increased attenuation.

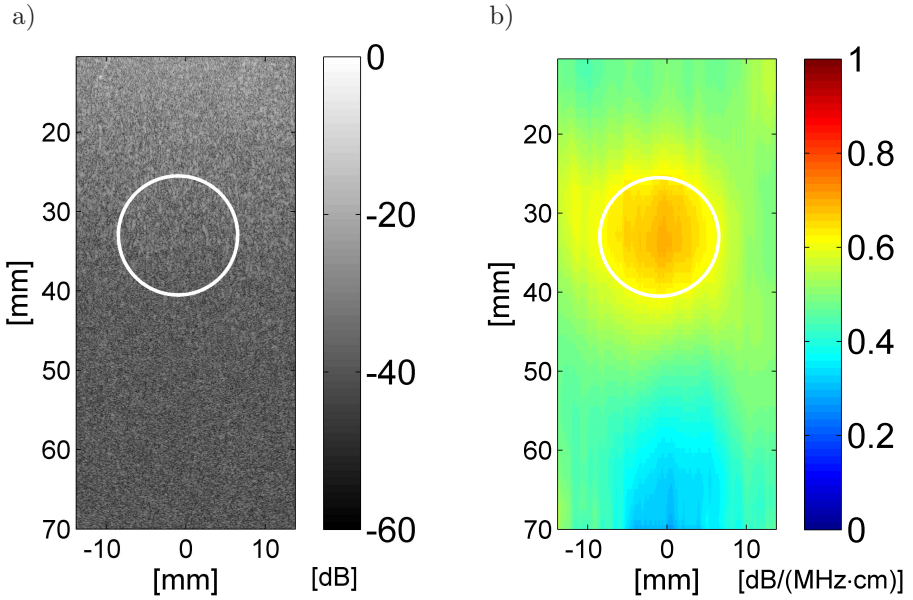

Fig. 5. B-scan image of the cylinder (attenuation 0.7 dB/MHz·cm) (a) and its attenuation distribution image (b). The white circles mark the real positions of cylinders. The shadows beneath the objects are artifacts and are caused by decreased signal-to-noise ratio (SNR) of echoes, due to increased attenuation.

6. Conclusions

Mean frequency correlation estimator and SSA technique were implemented for RF ultrasonic echoes processing in order to obtain the image of the attenuation map in tissue. The method was tested by simulation using the FieldII program. The new procedure enabling the simulation of the medium with non-uniform attenuation was implemented. The virtual tissue phantom containing the cylinder of 0.9 dB/(MHz·cm) attenuation immersed in medium of 0.5 dB/(MHz·cm) attenuation was created. The data collected by 64-element linear probe were simulated. The attenuating object is invisible on B-mode image, while it is visible on attenuation distribution image. The value of the estimated attenuation value was close to the assumed value. Next, the SA technique was tested using ultrasonic scanner and the tissue mimicking phantom. The estimated attenuation values were equal to 0.7 and 0.9 dB/(MHz·cm) and agreed well with the real attenuation. The images obtained in the measurements were better than the simulated ones. This was probably caused by the two times greater probe aperture comparing to the aperture assumed in simulations. We have found that the RF data obtained using synthetic aperture technique (SA) were much more reliable considering attenuation extraction then the echoes recorded applying DAS beamforming. The imaging of attenuation in tissue seems to be promising technique in medical diagnostics, however the precision of a single scan is often unsatisfactory. The synthetic transmit aperture technique allows to obtain the similar quality images as spatial compounding technique that utilize a dozen or so images for averaging (Klimonda *et al.*, 2010). The SA technique uses a single scan only, being more suitable for the real time application.

References

1. Bigelow T.A., McFarlin B.L., O'Brien W.D., Oelze M.L. (2008), *In vivo ultrasonic attenuation slope estimates for detectiong cervical ripening in rats: Preliminary results*, Journal of Acoustical Society of America, **123**, 3, 1794–1800.
2. Curlander J.C., McDonough R.N. (1991), *Synthetic aperture radar systems and signal processing*, John Wiley&Sons, New York.
3. Hassani H. (2007), *Singular Spectrum Analysis: Methodology and Comparison*, Journal of Data Science, **5**, 239–257.
4. Jensen J.A. (1996), *Field: A Program for Simulating Ultrasound Systems*, Paper presented at the 10th Nordic-Baltic Conference on Biomedical Imaging Published in Medical & Biological Engineering & Computing, pp. 351–353, **34**, Supplement 1, Part 1.
5. Jensen J.A., Svendsen N.B. (1992), *Calculation of pressure fields from arbitrarily shaped, apodized, and excited ultrasound transducers*, IEEE Trans. Ultrason., Ferroelec., Freq. Contr., **39**, 262–267.
6. Klimonda Z., Litniewski J., Nowicki A. (2009), *Spatial Resolution of Attenuation Imaging*, Archives of Acoustics, **34**, 4, 461–470.

7. Klimonda Z., Litniewski J., Nowicki A. (2010), *Tissue attenuation estimation from backscattered ultrasound using spatial compounding technique – preliminary results*, Archives of Acoustics, **35**, 4, 643–651.

8. Laugier P., Berger G., Fink M., Perrin J. (1985), *Specular reflector noise: effect and correction for in vivo attenuation estimation*, Ultras. Imag. **7**, 277–292.

9. Litniewski J. (2006), *Assessment of trabecular bone structure deterioration by ultrasound* [in Polish: *Wykorzystanie fal ultradźwiękowych do oceny zmian struktury kości gąbczastej*], IPPT Reports, No. 2.

10. Litniewski J., Klimonda Z., Lewandowski M., Nowicki A., Szymańska E. (2009), *Correcting for Focusing when Estimating Tissue Attenuation from Mean Frequency Shift*, IEEE International Ultrasonics Symposium Proceedings, 2383–2385.

11. Lu Z.F., Zagzebski J., Lee F.T. (1999), *Ultrasound Backscatter and Attenuation in Human Liver With Diffuse Disease*, Ultrasound in Med. & Biol., **25**, 7, 1047–1054.

12. McFarlin B.L., Bigelow T.A., Laybed Y., O'Brien W.D., Oelze M.L., Abramowicz J.S. (2010), *Ultrasonic attenuation estimation of the pregnant cervix: a preliminary results*, Ultrasound in Obstetrics and Gynecology, **36**, 218–225.

13. Oosterveld B.J, Thijssen J.M., Hartman P.C., Romijn R.L., Rosenbusch G.J. (1991), *Ultrasound attenuation and texture analysis of diffuse liver disease: methods and preliminary results*, Phys. Med. Biol., **36**, 8, 1039–1064,.

14. Saijo Y., Sasaki H. (1996), *High Frequency Acoustic Properties of Tumor Tissue*, [in:] *Ultrasonic Tissue Characterization*, Dunn F., Tanaka M., Ohtsuki S., Saijo Y. [Eds.], 217–230, Springer-Verlag Tokio, Hong-Kong.

15. Worthington A.E., Sherar M.D. (2001), *Changes in Ultrasound Properties of Porcine Kidney Tissue During Heating*, Ultrasound in Med. & Biol., **27**, 5, 673–682.

16. Zderic V., Keshavarzi A., Andrew A.M., Vaezy S., Martin R.W. (2004), *Attenuation of Porcine Tissues In Vivo After High Intensity Ultrasound Treatment*, Ultrasound in Med. & Biol., **30**, 1, 61–66.